Available online at www.sciencedirect.com
SCIENCE DIRECT®
Chemical Physics Letters 383 (2004) 304–308
CHEMICAL PHYSICS LETTERS
www.elsevier.com/locate/cplett

Theoretical study on the reaction path dynamics and rate constants for the hydrogen-abstraction reaction of atomic O (^{3}P) with CH_2FCl

Qingzhu Zhang *, Yueshu Gu, Shaokun Wang

School of Chemistry and Chemical Engineering, Shandong University, Jinan 250100, PR China

Received 20 October 2003; in final form 11 November 2003

Abstract

The hydrogen abstraction reaction of atomic O (^{3}P) with CH_2FCl has been studied theoretically for the first time. Geometries have been optimized at the MP2 level with the 6-311G(d, p) basis set. Energies along the minimum energy path have been improved by a series of single-point ab initio G3(MP2)//MP2/6-311G(d, p) calculation. The rate constants are obtained using canonical variational transition state theory (CVT) with small-curvature tunneling (SCT) correction method over a wide temperature range of 200–3000 K. The calculated results are compared with the available experimental values.

1. Introduction

The importance of haloalkanes in atmospheric chemistry is well-established [1–3]. To make the incineration of industrial wastes more efficient and less hazardous, it is necessary to understand all aspects of this combustion process. Basic understanding of the incineration mechanism is especially important in the case of haloalkanes, whose burning has the potential to generate products such as phosgene which are more hazardous than haloalkanes themselves. Reactions of atomic O (^{3}P) with haloalkanes are important initial steps of haloalkanes combustion [4].

Experimentally, the reactions of O (^{3}P) with haloalkanes have been extensively studied [5–11]. The extensive experimental literature contrasts with the lack of theoretical studies. As far as we know, only four theoretical reports are on record. Wang et al. [12] and Kreye [13] studied theoretically the mechanism and rate constants for the reactions of O (^{3}P) with CH_3F, CH_2F_2 and CHF_3. In two previous contributions from this laboratory [14,15] we presented theoretical rate constants for the reactions of O (^{3}P) with CH_3Br and CHF_2Cl. As part of our ongoing work in this field, this Letter investigates theoretically the kinetics properties for the reaction of O (^{3}P) with CH_2FCl. We have first revealed the reaction mechanism. In a second step, we have carried out the kinetics calculation using a 'direct dynamics' method [16] and by describing the chemical reaction using ab initio information (energies, gradients, and Hessians) only in the region of configuration space along the reaction-path.

2. Computation methods

By means of the GAUSSIAN 98 program [17], high-level ab initio calculations are carried out. First, the geometrical parameters and frequencies of the reactant, saddle point and products were calculated at the MP2/6-311G(d, p) level. Since unrestricted Hartree–Fock (UHF) reference wavefunctions are spin eigenfunctions for open-shell species, we monitored the expectation values of $\langle S^2 \rangle$ in the MP2/6-311G(d, p) optimization. Values of $\langle S^2 \rangle$ are 0.759 for the product CHFCl and for the transition state. After spin annihilation, the values of $\langle S^2 \rangle$ are 0.750 for CHFCl and 2.000 for the transition

* Corresponding author. Fax: +531-8564464.
E-mail address: guojz@icm.sdu.edu.cn (Q. Zhang).

0009-2614/$ - see front matter © 2003 Elsevier B.V. All rights reserved.
doi:10.1016/j.cplett.2003.11.044

state, which are the exact values for a pure doublet and for a pure triplet. Thus, spin contamination is not severe. In order to improve the energetic description of the stationary points, a series of single-point calculation was carried out at the G3(MP2) level [18]. In a second step, at the MP2/6-311G(d, p) level, the minimum energy paths (MEP) were constructed, starting from the, respectively, saddle point geometries and going downhill to both the asymptotic reactant and product channel with a gradient step size of 0.02 $amu^{1/2}$ bohr. Finally, the force constant matrices of the stationary points and selected non-stationary points near the saddle point along the MEP were also calculated.

To obtain kinetics information, we perform a canonical variational transition state theory calculation [19–21] with tunneling contributions included via a transmission coefficient. The kinetics calculation has been carried out using the POLYRATE 7.8 program [22]. The rotational partition functions were calculated classically, and the vibrational modes were treated as quantum-mechanical separable harmonic oscillators. In calculating electronic partition functions, we included the spin–orbit splitting of O (^{3}P), $^3P_0$, $^3P_1$ and $^3P_2$. Only the centrifugal-dominant small-curvature tunneling effect [23] correction method was used in our calculation of the rate constant. Methods for large curvature cases have been developed [24], but they require more information about the PES than was determined in the present study.

3. Result and discussion

The optimized geometries of the reactant, saddle point, and products are shown in Fig. 1. The vibrational frequencies of the reactant, products, and saddle point are listed in Table 1. Fig. 2 shows the classical potential energy (V_{MEP}) and vibrationally adiabatic potential energy (V_a^G) curves as functions of distance along the reaction coordinate s at the G3(MP2)//MP2/6-311G(d, p) level. Change curves of generalized normal-mode vibrational frequencies with the reaction coordinate s are shown in Fig. 3. The calculated TST, CVT, and CVT/SCT rate constants along with the experimental values are presented in Fig. 4 over the temperature range of 200–3000 K.

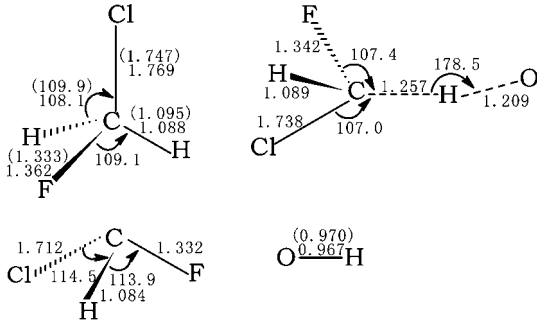

Fig. 1. MP2/6-311G(d, p) optimized geometries for the stationary points. Distances are in angstrom, and angles are in degree. The values in parenthesis are experimental data [25].

Table 1
The calculated vibrational frequencies (in cm^{-1}) and the zero-point energies (in kcal/mol) for the reactant, products, and saddle point involved in the reaction of O (^{3}P) with CH_2FCl at the MP2/6-311G(d, p) level

Species	Frequencies	ZPE
CH_2FCl	3228 3146 1526 1439 1297 1120 1044 799 398 *3048 2993 1468 1351 1236 1068 1001 760 385*	20.01
TS	3185 1388 1293 1188 1160 996 847 563 402 167 100 2557i	16.13
CHFCl	3242 1361 1201 900 804 420	11.33
OH	3852 *3735*	5.51

The values in italics are the experimental data [26].

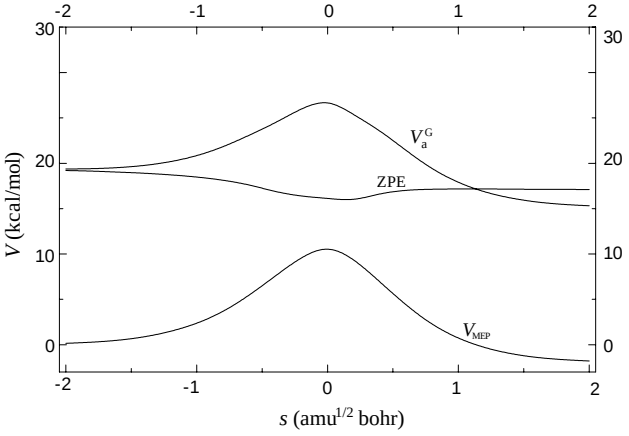

Fig. 2. The potential energy (V_{MEP}) and vibrationally adiabatic potential energy (V_a^G) curves as functions of s at the G3(MP2)//MP2/6-311G(d, p) level for the reaction of O (^{3}P) with CH_2FCl.

3.1. Reaction mechanism

Fig. 1 and Table 1 show the geometric parameters and frequencies of the reactant and products at the MP2/6-311G(d, p) level along with the available experimental data. It can be seen from Fig. 1 that the geometric parameters of CH_2FCl and OH optimized are in good agreement with the experimental values. The vibrational frequencies of CH_2FCl and OH agree well with the experimentally observed fundamentals, and the maximum relative error is less than 7%. These good agreements give us confidence that the MP2/

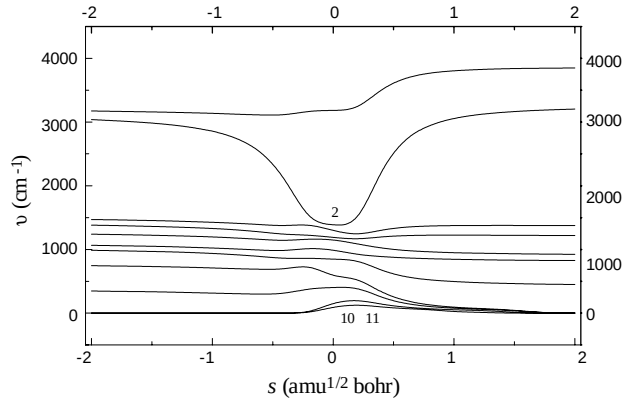

Fig. 3. Changes of the generalized normal-mode vibrational frequencies as functions of s at the MP2/6-311G(d, p) level for the reaction of O (^{3}P) with CH_2FCl.

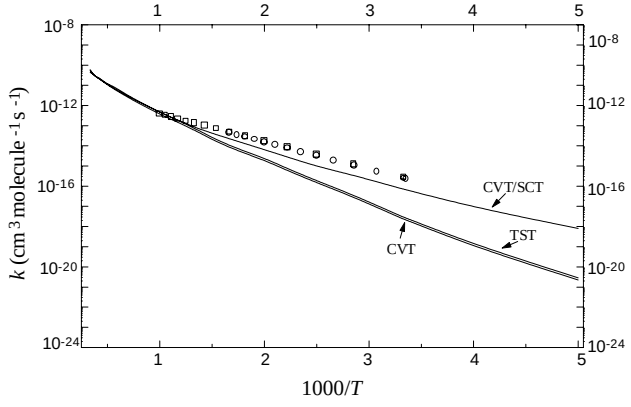

Fig. 4. Arrhenius plot of the rate constants in the temperature range of 200–3000 K for the reaction of O (^{3}P) with CH_2FCl. (□) and (○) are the experimental values [10,11].

6-311G(d, p) theory level is adequate to optimize the geometries and calculate the frequencies.

The reactions of O (^{3}P) with haloalkanes are the prototype of simple metathesis reactions in which a hydrogen atom is transferred via an apparent barrier in the reaction coordinate. For the reactions of O (^{3}P) with CH_3F, CH_2F_2, CHF_3, CH_3Br and CHF_2Cl [12–15], the approach of the O (^{3}P) to C–H bond with C_s symmetry proceeds over two potential energy surfaces (PESs), $^3A' + {}^3A''$ by the Jahn–Teller effect. Due to having lower symmetry (C_1 symmetry) in the saddle point structure, the Jahn–Teller effect was not found in the reaction of O (^{3}P) with CH_2FCl. Indeed, for C_1 symmetry the irreducible representation is ^3A for reactants and $^3A + {}^1A$ (2) for products, and therefore, both asymptotes adiabatically correlate through the PES ^3A in C_1. At the MP2/6-311G(d, p) level, a saddle point with the C_1 symmetry was located for the reaction of O (^{3}P) with CH_2FCl, its geometrical structures are shown in Fig. 1. The breaking C–H bond is elongated by 15.53%, while the forming O–H bond is longer than the equilibrium value of 0.967 Å by 25.03%. Therefore, the saddle point is reactant-like. The saddle point is identified with one negative eigenvalue of the respective Hessian matrix and, therefore, one imaginary frequency. Since the imaginary frequency governs the width of the classical potential energy barrier along the MEP, it plays an important role in the tunneling calculations, especially when the imaginary frequency is large, and the associated eigenvector has a large component of hydrogenic motion. For the title reaction, the imaginary frequency of the saddle point is 2557i, so we expect that the tunneling effect should be important for the calculation of the rate constant. Direct inspection of the saddle point low-frequency mode indicates that the mode of the lowest frequency is a hindered internal rotation instead of a small-amplitude vibration. The mode was removed from the vibrational partition function for the saddle point and the corresponding hindered rotor partition function $Q_{HR}(T)$, calculated by the method devised by Truhlar [27], was included in the expression of the rate constant. For the transition state, the HOMO–LUMO gap of the reaction of O (^{3}P) with CH_2FCl is less than that of O (^{3}P) with CH_4.

In order to choose a reliable theory level to calculate the energy, the C–H bond dissociation energy was calculated at various levels for the CH_2FCl. The experiment gave the spectroscopic dissociation energy, and so the calculated dissociation energies were corrected for the ZPE. The calculated result of 98.39 kcal/mol at the G3(MP2) level is in good agreement with the experimental value of 100.8 kcal/mol [28], especially if the experimental uncertainty (± 1.3 kcal/mol) is taken into consideration. Therefore, the G3(MP2) level is a good choice to calculate accurate energies for the title system. At the G3(MP2) level, the potential barrier and reaction enthalpy of the reaction of O (^{3}P) with CH_2FCl are 10.97 and −1.93 kcal/mol.

3.2. The kinetics calculation

3.2.1. Reaction path properties

The minimum energy path (MEP) was calculated at the MP2/6-311G(d, p) level by the IRC definition, and the energies of the MEP was refined by the G3(MP2)//MP2 level. For this reaction, the maximum position of the classical potential energy V_{MEP} curve at the G3(MP2)//MP2 level corresponds to the saddle point structure at the MP2/6-311G(d, p) level. Therefore, the shifting of the maximum position for the V_{MEP} curve caused by the computational technique is avoided (avoiding artificial variational effect). The changes of the classical potential energy V_{MEP} and the ground-state vibrational adiabatic potential energy V_a^G with the reaction coordinate s are shown in Fig. 2. The V_{MEP} and V_a^G curves are similar in shape, and their maximum

positions are almost the same at the G3(MP2)//MP2 level. It means that the variational effect will be small for this title reaction. The zero-point energy ZPE, which is the difference of V_a^G and V_{MEP}, is also shown in Fig. 2. The zero-point energy curve is almost unchanged as s varies except that only from $s = -1.0$ to 1.0 amu$^{1/2}$ bohr there is a little valley. In order to analyze this behavior in greater detail, we show the variation of the generalized normal modes vibrational frequencies, which were calculated by using Cartesian coordinates, in Fig. 3.

In the negative limit of s, the frequencies are associated with the reactants ($CH_2FCl + O$), while in the positive limit of s, the frequencies are associated with the products ($CHFCl + OH$). The vibrational mode 2 (reactive mode) that connects the frequency of C–H stretching vibration in CH_2FCl with the frequency of the O–H stretching vibration of OH drops dramatically from $s = -1.0$ to $s = 1.0$ amu$^{1/2}$ bohr, this behavior is similar to that found in other hydrogen abstraction reactions [29,30]. If changes in other frequencies were small, this drop could cause a considerable fall in the zero-point energy near the saddle point. The two lowest harmonic vibrational frequencies (modes 10 and 11, transitional modes) along the reaction path correspond to the transformation of free rotations or free translations of the reactant limit into real vibrational motions in the global system. Their frequencies tend asymptotically to zero at the reactant and product limits, and reach their maximum in the saddle point zone. Therefore, in the saddle point region, the behavior of these transitional modes partially compensates the fall in the zero-point energy caused by mode 2. As a result, the zero-point energy curve shows a little drop in the saddle point zone.

3.2.2. The rate constant

The canonical variational transition state theory (CVT) with a small-curvature tunneling correction (SCT), which has been successfully performed for several analogous reactions [31,32], is an efficient method to calculate the rate constant. In this Letter, we used this method to calculate the rate constants for the reaction of O (^{3}P) with CH_2FCl over a wide temperature range from 200 to 3000 K.

In order to calculate the rate constant, 30 points were selected near the saddle point along the MEP, 15 points in the reactant zone and 15 points in the product zone. Fig. 4 shows the calculated rate constants along with the experimental values against the reciprocal of the temperature for the reaction of O (^{3}P) with CH_2FCl over the temperature range of 200–3000 K. For the purpose of comparison, the conventional transition state theory (TST) rate constants and the variational transition state theory (CVT) rate constants without the tunneling correction are also shown Fig. 4. Several important features of the calculated rate constants are the following:

(1) It can be seen that the rate constants of TST and CVT are nearly the same in the whole studied temperature range of 200–3000 K, which enables us to conclude that the variational effect is small for the calculation of the rate constant. It is in accordance with the above analysis.

(2) Reactions involving hydrogen atom transfer are usually characterized by a significant tunneling effect that must be accounted for when computing reaction rate constants. In the present case, the CVT/SCT rate constants are greater than the CVT ones over the temperature range of 200–800 K. For example, at 298 K, the CVT rate constant is 2.13×10^{-18} cm^3 molecule^{-1} s^{-1}, while the CVT/SCT rate constant is 6.68×10^{-17} cm^3 molecule^{-1} s^{-1}. The latter is 31.4 times larger than the former. The difference between the CVT rate constant and the CVT/SCT rate constant decreases with the increase in temperature. When the temperature is higher than 900 K, the CVT/SCT rate constants are asymptotic to the rate constants of CVT, which means only in the lower temperature range the small-curvature tunneling correction plays an important role for the calculation of the rate constant. The contribution of tunneling becomes progressively less important as the temperature rises.

(3) In the temperature range of 500–1000 K, the CVT/SCT rate constants deviate from the corresponding experimental values by no more than a factor of 2, and the CVT/SCT rate constants are in much better agreement with the experimental values. In the temperature range of 298–400 K, the calculated CVT/SCT rate constants are slightly smaller than the values obtained from the experimental Arrhenius expression fitted by Jourdain et al. [10] and Herron [11]. For example, at 298 K, the CVT/SCT rate constant is 6.68×10^{-17} cm^3 molecule^{-1} s^{-1}, while the experimental value is 2.21×10^{-16} cm^3 molecule^{-1} s^{-1}. The experimental value is about a factor of 3.3 larger than the theoretical rate constant. Certainly, those earlier experimental results may not be conclusive because in this temperature range the rate constant is so small that it is very difficult to obtain an accurate experimental value. The observed discrepancy between the theoretical rate constants and the experimental values at low temperature could also be due to an underestimate of the tunneling factor and it is possible that a more sophisticated method for its estimated than the SCT method could reduce the differences. For example, for the similar $CH_4 + O$ reaction [33], rate constants calculated using the SCT method and an optimized multidimensional method for tunneling differ by a factor of 18 at 300 K, the later being closer to the experimental values than the former.

(4) The calculated rate constants exhibit typical non-Arrhenius behavior. The rate constants of the title reaction are fitted by three-parameter formulas over the

temperature range of 200–3000 K and given in units of cm^3 $molecule^{-1}$ s^{-1} as follows:

$$k(T) = 6.09 \times 10^{-17} T^{1.88} \exp(-4057.50/T),$$

for TST rate constants,

$$k(T) = 1.18 \times 10^{-17} T^{2.07} \exp(-3972.39/T),$$

for CVT rate constants,

$$k(T) = 2.47 \times 10^{-21} T^{3.06} \exp(-2133.71/T),$$

for CVT/SCT rate constants.

(5) At low temperature, the rate constants for the reaction of O (^3P) with CH_2FCl are relatively small. Therefore, this reaction can not occur to any significant extent under the atmospheric condition. However, the rate constants increase rapidly with elevation of temperature. At 3000 K, the rate constant of the reaction is 4.50×10^{-11} cm^3 $molecule^{-1}$ s^{-1}. So the reaction should play an important role under high-temperature combustion conditions.

4. Conclusion

In this Letter, we studied the reaction of O (^3P) with CH_2FCl using ab initio and canonical variational transition state theory (CVT) with small-curvature tunneling effect. Rate constants were reported over the temperature range of 200–3000 K. Several major conclusions can be drawn from this calculation.

1. This reaction proceeds via a direct hydrogen abstraction mechanism.
2. The calculated rate constants exhibit typical non-Arrhenius behavior.
3. In the temperature range of 500–1000 K, the calculated CVT/SCT rate constants are in good agreement with the experimental values. In the temperature range of 298–400 K, the calculated rate constants are slightly smaller than the experimental values.

Acknowledgements

The authors thank Professor Donald G. Truhlar for providing the POLYRATE 7.8 program. This work is supported by the Research Fund for the Doctoral Program of Higher Education of China.

References

[1] R. Tuck, A. Plumb, E. Condon, Geophys. Res. Lett. 17 (1990) 313.
[2] L. Manzer, Science 249 (1990) 31.
[3] R. Atkinson, Chem. Rev. 86 (1986) 69.
[4] J.I. Warnatz, in: W.C. Gardiner Jr. (Ed.), Combustion Chemistry, Spinger-Verlag, New York, 1984.
[5] K.M. Smith, G. Duxburg, D.A. Newnham, J. Ballard, J. Chem. Soc. Faraday Trans. 93 (1997) 2735.
[6] A.W. Miziolek, W. Tsang, in: Halon Replacements: Technology and Science, ACS Symposium Series, 611, American Chemical Society, Washington, DC, 1995.
[7] M. Kneba, J. Wolfrum, Ber. Bunsenges, Phys. Chem. 81 (1977) 1275.
[8] M.-C. Su, K.P. Lim, J.V. Michael, J. Phys. Chem. 98 (1994) 8411.
[9] A.A. Westenberg, N. DeHaas, J. Chem. Phys. 62 (1975) 4477.
[10] J.L. Jourdain, G. Poulet, J. Barassin, G. LeBras, J. Combourieu, Pollut. Atmos. 75 (1977) 256.
[11] J.T. Herron, J. Phys. Chem. Ref. Data 17 (1988) 967.
[12] B.-S. Wang, H. Hou, Y.-S. Gu, Chem. Phys. 247 (1999) 201.
[13] W.C. Kreye, Chem. Phys. Lett. 256 (1996) 383.
[14] Q.-Z. Zhang, S.-K. Wang, Y.-S. Gu, Chem. Phys. Lett. 352 (2002) 521.
[15] Q.-Z. Zhang, Y.-S. Gu, S.-K. Wang, J. Phys. Chem. (2003), proof.
[16] D.G. Truhlar, M.S. Gordon, Science 249 (1990) 491.
[17] M.J. Frisch et al., GAUSSIAN 94, Revision E.1, Gaussian, Pittsburgh, PA, 1995.
[18] L.A. Curtiss, P.C. Redfern, K. Raghavachari, V. Rassolov, J.A. Pople, J. Chem. Phys. 110 (1999) 4703.
[19] K.K. Baldridge, M.S. Gordon, R. Steckler, D.G. Truhlar, J. Phys. Chem. 93 (1989) 5107.
[20] A. Gonzalez-Lafont, T.N. Truong, D.G. Truhlar, J. Chem. Phys. 95 (1991) 8875.
[21] B.C. Garrett, D.G. Truhlar, J. Phys. Chem. 83 (1979) 1052.
[22] R. Steckler et al., POLYRATE, Version 7.8, University of Minnesota, Minneapolis, 1997.
[23] Y.-P. Liu, G.C. Lynch, T.N. Truong, D.-H. Lu, D.G. Truhlar, B.C. Garrett, J. Am. Chem. Soc. 115 (1993) 2408.
[24] T.N. Truong, D.-H. Lu, G.C. Lynch, Y.P. Liu, V.S. Melissas, J.J. Stewart, R. Steckler, B.C. Garrett, A.D. Isaacson, A. Gonzalez-Lafont, S.N. Rai, G.C. Hancock, T. Joseph, D.G. Truhlar, Comput. Phys. Commun. 75 (1993) 43.
[25] M.P. Harmony, V.W. Laurie, R.L. Ramsay, F.J. Lovas, W.J. Lafferty, et al., J. Phys. Chem. Ref. Data 8 (1979) 619.
[26] JANAF, vol. 14 (Suppl. 1), 1985.
[27] D.G. Truhlar, J. Comput. Chem. 12 (1991) 266.
[28] D.R. Lide (Ed.), CRC Handbook of Chemistry and Physics, 78th ed., CRC Press, New York, 1997–1998.
[29] J. Espinosa-Garcia, J.C. Corchado, J. Phys. Chem. 100 (1996) 16561.
[30] J.C. Corchado, J. Espinosa-Garcia, J. Chem. Phys. 106 (1997) 4013.
[31] J. Espinosa-Garcia, J. Phys. Chem. A 104 (2000) 7537.
[32] V.S. Melissas, D.G. Truhlar, J. Chem. Phys. 99 (1993) 1013.
[33] J.C. Corchado, J. Espinosa-Garcia, O. Roberto-Neto, Y.-Y. Chuang, D.G. Truhlar, J. Phys. Chem. A 102 (1998) 4899.